Title
Fault Stability Perturbation by Thermal Pressurization and Stress Transfer Around a Deep Geological Repository in a Clay Formation

Journal
Journal of Geophysical Research: Solid Earth, 124(8)

ISSN
2169-9313

Authors
Urpi, L
Rinaldi, AP
Rutqvist, J
et al.

Publication Date
2019-08-01

DOI
10.1029/2019jb017694

Peer reviewed

Fault Stability Perturbation by Thermal Pressurization and Stress Transfer Around a Deep Geological Repository in a Clay Formation

L. Urpi[1], A. P. Rinaldi[1], J. Rutqvist[2], and S. Wiemer[1]

[1] Swiss Seismological Service, ETH Zürich, Zürich, Switzerland, [2] Energy Geoscience Division, Lawrence Berkeley National Laboratory, Berkeley, CA, USA

Correspondence to: L. Urpi, luca.urpi@pm.me

Abstract

The increase of temperature of a low-permeability, fluid-saturated media may trigger significant thermal pressurization, where the expansion of pore fluid cannot be accommodated by the thermal expansion of the pore space. With the aid of a coupled thermohydromechanical numerical simulator, we investigate the possible impact of thermal pressurization during the life of a deep geological repository (DGR) for high-level radioactive waste, characterized by the emplacement of radioactive material-filled canisters in a series of parallel tunnels, excavated in a low-permeability clay formation. We represent the fault as a planar structure embedded in a thermoporoelastic material and shear activation evaluated by a strain-softening Mohr-Coulomb failure criterion. The results show that stress changes caused by temperature and thermal pressurization of a rock mass around the emplacement tunnels may trigger a slip event on a fault plane in proximity of the geological disposal site: Rupture nucleates at depth, hundreds of meters below the DGR. Stress transfer plays a key role, while a direct hydraulic connection between the repository and the nucleation zone is not necessary in order to trigger rupture. A low stress ratio may favor the occurrence of slip up to a distance of 600 m of the fault from the outermost tunnel. These results highlight the need of investigating hydromechanical properties and local stress conditions at depth to characterize the geomechanical response of weak planes located in the surroundings of a high-level radioactive waste repository and to provide sufficient knowledge for the safe development of the DGR site.

1 Introduction

A safe geological disposal site of radioactive waste requires identification of a rock formation that guarantees isolation to prevent unacceptable concentrations of radionuclides from migrating to the accessible environment. Among the favorable properties for a disposal in clay formations include (i) minimal diffusion of radionuclides, (ii) low hydraulic conductivity, and (iii) the capacity for self-sealing. The self-sealing capacity is particularly important to recover intactness of the excavation damage zone generated during the tunneling activities to construct the disposal site. Among the possible clay materials, the one found in the Opalinus Clay formation in northern Switzerland has been intensively investigated (Bossart,

Bernier, et al., 2017). Opalinus Clay is an example of an argillaceous clay formation resulting from specific tectonic processes, featuring a highly consolidated material with porosity up to 14–16% and extremely low permeability, on the order of 10^{-20}–10^{-21} m^2 (Horseman et al., 1996). Currently, a common design for spent nuclear fuel disposal is the excavation of a series of horizontal tunnels to be filled with specifically engineered canisters containing vitrified high-level radioactive waste that are embedded within a buffer of swelling (bentonite-based) clay. Given the low permeability of a clay host formation, we can reasonably assume that near undrained conditions will be reached, even for relatively slow strain rate. Notwithstanding the background tectonic strain, the increase in temperature in the canisters and in the surrounding region due to the decaying radioactive material represents a local mechanism capable of straining the rock mass significantly. A side effect of the temperature increase in a low-permeability porous material has been described analytically by Palciauskas and Domenico (1982): In their work they showed that a continuously heated low-permeability, fluid-saturated poroelastic material will undergo an increase of the pore pressure, if the hydraulic diffusivity is much lower than the thermal diffusivity. The causative mechanism lies in the difference between the thermal expansivity coefficients of the fluid and the solid phase, responsible for a larger increase in fluid volume with respect to the volumetric expansion of the pore space. The near undrained conditions under which the media is found would then prevent or strongly impede the excess fluid volume from flowing to reequilibrate the pressure gradient.

Recently, thermal pressurization (also known as thermal pore pressure) has been observed in northern Alberta, Canada, during the extraction of steam-heated heavy oil (Xu et al., 2013). After the Athabasca heavy oil reservoir formation was treated with the injection of steam at a pressure of up to 2 MPa, the overlying low-permeability Wabiskaw sands intervals, acting as a caprock for the reservoir, showed an increase of pore pressure up to 6 MPa, measured some months after the steam injection during the drilling of a new borehole. No evidence of a hydraulic connection between the two formations or degradation of the sealing capacity of the caprock was found, and numerical analysis performed by Xu et al. (2013) showed that this pressurization is consistent with thermal pore pressure generation induced by the hot steam.

Thermal pressurization is a plausible mechanism responsible for the massive collapse of stratovolcanoes (Reid, 2004). In this scenario, a remote, deep magma intrusion leads to the elevation of the pore pressure of a shallow hydrothermal system, without a direct interaction with the hot molten material and the fluid-saturated shallow formations. Consequently, the perturbation of effective stress and the degradation of mechanical properties due to the thermal pressurization will lead to the collapse of the volcanic edifice.

In the seismological community, thermal pressurization can be found as a consequence of shear slip, capable of preventing the melting of shearing material (Rempel & Rice, 2006; Sibson, 1973) and leading to an enhancement of slip weakening mechanism that causes the rupture to propagate farther and faster (Schmitt et al., 2011). The occurrence and importance of thermal pressurization as a slip weakening mechanism during shallow events is discussed extensively in Chen et al. (2017): Their study shows that, with increasing permeability, the thermal pressurization weakening effects is complemented by the vaporization of fault water, which buffers the possible temperature increase as well as further reducing the dynamic friction coefficient.

In agreement with the analytical description by Palciauskas and Domenico (1982), thermal pressurization has been observed in clay materials both at the laboratory and at the field scale, from the centimeter-size samples obtained from the Opalinus Clay formation (Zhang et al., 2017) to the results of a field test with a 1:1-scale heater experiment at the underground research laboratory in Mont Terri, Switzerland (Bossart, Jaeggi, & Nussbaum, 2017). The field test showed that in situ pressure of up to 4 MPa has been reached as a result of an increase in temperature of 30 °C. Theoretically, a bound on maximum possible overpressure is given by the sum of the combined in situ minimum stress and the tensile strength of the rock. If pore pressure reaches this threshold value, new pore space will be created by tensile opening and fluid will be able to move into it, and consequently, the hosting rock will at least temporarily lose its sealing capacity.

Assuming that the layout of the geological disposal repository will be a series of parallel emplacement tunnels filled with heat-releasing waste canisters, a relevant volume of the rock mass hosting the repository will be subject to an increase in temperature. The thermoelastic stresses and their impact on stability of faults and fractures for a deep geological repository built in a fractured crystalline formation have been investigated by Min et al. (2013). They showed that shearing of faults and fractures is possible. The fractured nature of the crystalline formation should prevent the buildup of thermal pore pressure, so groundwater flow perturbation would occur only in relation to permeability changes induced by the repository activity. In a clay formation the thermal pressurization will not have hydrological relevance, since a clay formation is expected to behave as an aquiclude (not affecting the regional groundwater flow). However, thermal pressurization can enhance thermoelastic effects, such as a reduction of vertical stress and associated deformations affecting the surface and/or the underground structures (Read, 2002) as well as potentially leading to destabilization of faults located at a distance from the repository. Several studies show that a fault reactivation could be associated with the injection of relatively small amount of fluids, sometime even leading to human-felt events in seismological quiet areas. Examples are the stimulation of a shale gas well in the United Kingdom (Clarke et al., 2014), during the initial phases of the

offshore Castor gas storage project, Eastern Spain (Cesca et al., 2014), as well as in more seismic prone areas like Switzerland, where human-felt events were triggered during the stimulation of the Basel geothermal reservoir (Deichmann & Giardini, 2009) and during the St. Gallen geothermal project (Diehl et al., 2017).

In this work, we model the first centuries of operation of a generic underground repository filled with heat-decaying radioactive material. We investigate if the induced stress and thermal perturbation (in terms of stress, pore pressure, and temperature) can propagate outside the disposal formation and trigger the reactivation of a fault located in the proximity of the repository. We explored the influence of fault-tunnel distance, horizontal to vertical stress ratio, and fault cohesion to assess their influence on the occurrence and extent of the rupture.

2 Laboratory and Field Evidence of Thermal Pressurization

Laboratory investigations carried out on Opalinus and Callovian-Oxfordian clay samples have shown an increase of pore pressure respectively of 8 and 11 MPa, due to an increase in temperature from 30 to 60 °C applied in undrained conditions (Zhang et al., 2017). Based on these results a thermal pressurization coefficient was computed to be on the order of 0.23 MPa/°C.

Previously, Monfared et al. (2011) reported for an Opalinus Clay sample an undrained pore pressure increase of 1.2 MPa due to an increase in temperature from 25 to 55 °C, corresponding to an average thermal pressurization coefficient of 0.05 MPa/°C. Ghabezloo and Sulem (2009) derived an analytical formulation of the coefficient of thermal pressurization Λ, by considering the porosity n_0, the thermal expansion coefficients of solid α_s and of fluid α_f and the compressibilities c_f, c_s, and c_d, respectively, of fluid, of solid grain, and of the drained porous media:

$$\Lambda = \frac{n_0(\alpha_f - \alpha_s)}{n_0(c_f - c_s) + (c_d - c_s)}. \quad (1)$$

Applying this formula to the thermoelastic properties for Opalinus Clay obtained by Muñoz (2007), thermal pressurization coefficient of 0.08 MPa/°C can be estimated.

In low-permeability argillaceous rock, the increase in pore pressure has been observed at the field scale during the Mont Terri HE-D experiment, where two heating devices were emplaced in a 30-cm-diameter canister. The heaters were provided 650 W of power for 90 days, subsequently the power was rapidly raised to 1,950 W for additional 248 days. Pore pressure and temperature were monitored at various boreholes drilled nearby the emplaced canisters (Wileveau, 2005). The sensors installed in the boreholes measured an increase in pore pressure with increasing temperature: Gens et al. (2007) clarified the coupling of thermal to hydraulic and mechanical effects, while Garitte et al. (2017) later provided a numerical benchmarking exercise to confirm the thermohydromechanical (THM) coupling effect. In a

recent numerical reproduction of the experiment, Nguyen (2018) noted that the maximum measured pressure of 4 MPa could be sufficient to create new tensile fractures in intact rock, given that the in situ minimum principal stress is estimated to be in the range of 2–3 MPa (Martin & Lanyon, 2003), while tensile strength of the Opalinus Clay is expected to be of the order of 1 MPa parallel to bedding and 0.5 MPa perpendicular to bedding (Bock, 2001). The thermal pressurization coefficient that can be derived from the in situ HE-D experiment is on the order of 0.1 MPa/°C. Table 1 summarizes estimates of the thermal pressurization coefficient for Opalinus and Callovian-Oxfordian clay under different conditions.

Table 1
Thermal Pressurization Coefficient Calculated for Opalinus and Callovian-Oxfordian Clay Under Different Conditions

Source	ΔT (°C)	ΔP (MPa)	Λ (MPa/°C)
Experiment (Monfared et al., 2011)	25 → 55	1.2	0.05
Experiment (Zhang et al., 2017)	30 → 60	8	0.23
Analytical (derived from Muñoz, 2007)	—	—	0.08
Field (Wileveau, 2005)	15 → 25	1	0.1

3 Coupled Geomechanical Model

We simulate a generic repository case with the coupled TOUGH-FLAC simulator (Rutqvist, 2017) to assess the influence of thermal, hydrogeological, and mechanical processes on the in situ stress state and on its distribution on a nearby plane of weakness.

The iteratively coupled TOUGH-FLAC code is based on linking the finite-volume code for multiphase flow and heat transport TOUGH2 (Pruess et al., 2012) with the finite-volume geomechanics software (ITASCA Consulting Group, Inc, 2012). Temperature and pressure distribution calculated by TOUGH2 are fed into the geomechanical simulator FLAC3D to calculate the stress state and to assess if failure conditions are reached. Thermal pressurization is computed in TOUGH2, being determined by the interplay between fluid thermal expansion, porosity change due to pressure and temperature, and the amount of water allowed to move by the formation permeability.

Plastic behavior is taken into account for an assumed nearby fault and for the bedding planes embedded in the disposal formation. Failure is calculated in accordance with the Mohr-Coulomb criterion, where the material will behave plastically if the shear stress overcomes the material strength. Shear and normal stresses are calculated from the stress tensor according to the plane of weakness orientation relative to the principal stresses. A similar approach has been used extensively to model the response of fault zones subjected to fluid injection (Cappa & Rutqvist, 2011; Rinaldi, Jeanne, et al.,

2014; Rinaldi, Rutqvist, & Cappa, 2014; Rutqvist et al., 2013) or extraction (Zbinden et al., 2017). Such a model can be further extended, to account for increasing complexity, being successfully applied also for a full 3-D formulation (e.g., Rinaldi et al., 2015; Rutqvist et al., 2015), as well as for studying the ground surface response by dynamic rupture modeling (Cappa & Rutqvist, 2012; Rinaldi, Jeanne, et al., 2014) and with slip rate-dependent friction evolution (Urpi et al., 2016).

In the study presented here, a known fault with 80° dip is located at 225-m distance from the outer emplacement tunnel, taking into account an empirical safety distance of 200 m arising from possible underestimation of a fault/fracture extension as imaged by geophysical methods (NAGRA, 2008). The fault cuts through the argillaceous formation where the emplacement tunnels are located, extending both through the units lying above and below the repository. The fault is embedded in a 2 × 2-km domain, defined in plane-strain condition. The medium is considered elastic, with the exception of the clay formation and the fault zone that are subjected to a plastic behavior upon reactivation. The properties of the formation (i.e., cohesion/friction and orientation of bedding) are determined based on available literature (NAGRA, 2016; te Kamp & Konietzky, 2005) to be representative of a repository located at 700-m depth. A scheme of the model is shown in Figure 1, with thermal, mechanical, and hydraulic properties are summarized in Table 2.

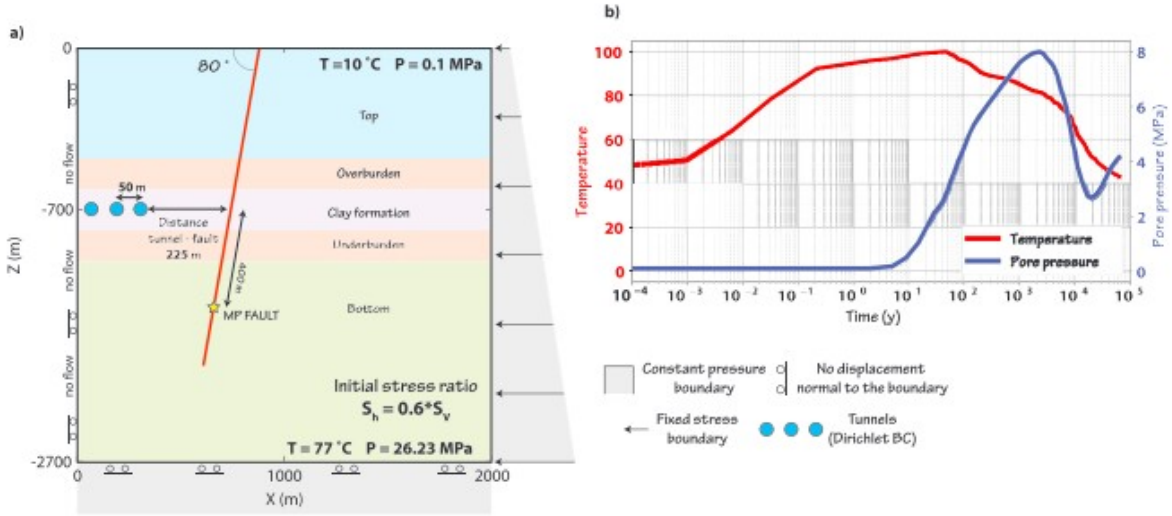

Figure 1. (a) Scheme depicting different units and boundary conditions. Not to scale, number of tunnels and their locations approximated for visualization purposes only. (b) Pressure and temperature derived from Rutqvist, Zheng, et al. (2014) for a radioactive canister having initial power of 200 W/m. Values calculated are for the interface between the engineered barrier system and the rock mass.

Table 2
Thermohydromechanical Properties for the Definition and Characterization of the Model

Parameter (unit)	Top	Overburden	Clay formation	Underburden	Bottom
Thickness (m)	550	75	150	75	1,150
Density (kg/m^3)	2,430	2,430	2,430	2,430	2,430
Young's mod. (GPa)	37	8	12.7	8	9
Poisson's ratio	0.27	0.27	0.2	0.27	0.27
Permeability (m^2)	10^{-18}	10^{-15}	$//3 \times 10^{-19}$ **T** 6×10^{-20}	10^{-15}	10^{-15}
Porosity (%)	10	10	7.4	10	1
Specific heat (J/Kg·°C)	920	920	920	920	920
Thermal conductivity (W/M/°C)	3.2	3.2	3.2	3.2	3.2
Thermal expansion coefficient (1/°C)	2.00×10^{-5}	2.00×10^{-5}	2.00×10^{-5}	2.00×10^{-5}	2.00×10^{-5}
Pore compressibility (1/Pa)			10^{-9}		
Pore expansivity (1/°C)			1.4×10^{-3}		
Mohr-Coulomb parameters (before/after rupture)	Clay beddings	Fault			
Dip	0	80			
Friction angle (°)	20/20	20/20			
Cohesion (MPa)	5.6/1.8	0.35/0			
Dilation angle (°)	0	0			

Note. Data from te Kamp and Konietzky (2005) and from Corkum and Martin (2007). Fault cohesion is subject of a sensitivity analysis in the range 0–1 MPa. For the clay formation the possibility of failure along bedding planes is considered (NAGRA, 2016).

In the repository formation, each tunnel is represented by a single element of size 3 × 3 m, which includes the canister, the bentonite buffer barrier, and the first decimeters of host rock. Representing the emplacement tunnel with a single element means that our model must rely on externally calculated curves for pressure and temperature, since it will lack the capability to resolve the processes taking place in the tunnel and at a close distance of the canisters. We rely on past development of the code, starting from the implementation of the Barcelona Basic Model (Alonso et al., 1990; Gens et al., 2006) into TOUGH-FLAC, and the consequent work of Rutqvist, Zheng, et al. (2014) where a comprehensive THM model of the emplacement tunnel-canister system was developed to investigate the near-field behavior in the rock mass. This work allows us to lump together the canister-tunnel behavior, providing the pressure and temperature internal boundary conditions of our THM simulation, to investigate the possible destabilization of a nearby fault not intersecting the repository. Rutqvist, Zheng, et al. (2014) calculated the thermal pressurization coefficient of 0.4 MPa/°C for a clay formation showing same properties described in the HE-D experiment (Gens et al., 2007).

Fault material properties are derived from the recent laboratory investigations performed by Orellana et al. (2018): Their results show that a Mohr-Coulomb criterion can be fitted to their observations, assuming a friction angle of about 20° and a cohesion value of 0.35 MPa for material

under a compressive normal stress of up to 4 MPa. In our model the friction angle is assumed to be strain neutral, while the cohesion drops to 0 as soon as the failure conditions are reached. The sensitivity investigation for cohesion has been performed in the range 0–0.95 MPa, assuming always a maximum cohesion drop of 0.35 MPa.

Normal tectonic regime is imposed by assigning appropriate initial stress conditions (horizontal minimum stress S_h is 0.6 times the vertical lithostatic stress S_v). Initially, the pressure profile is hydrostatic, with the disposal formation behaving as an aquiclude, a porous hydrogeological unit capable of storing water but not capable of transmitting it at an appreciable rate. A sensitivity analysis has been performed for stress ratio (S_h divided S_v) in the range 0.58–0.64.

Boundary conditions account for tectonic stresses applied to the lateral right boundary and free surface conditions at the top boundary. Roller boundary conditions (no displacement allowed in the directional perpendicular to the boundary) are applied to the left and bottom boundaries. Fixed pressure is imposed at the bottom and at the top of the model, while a no-flow boundary is applied on the left boundary.

In the simulations, the heating power is not directly included since temperature and pressure imposed as a source term are the one calculated by Rutqvist, Zheng, et al. (2014), based on 200 W of thermal power per meter of emplacement tunnel, with a center-to-center spacing of 50 m between each emplacement tunnel. The Dirichlet boundary conditions applied to mimic the tunnel and its complex behavior are derived directly from Rutqvist, Zheng, et al. (2014), and it is plotted in Figure 1b. Our simulation stops when rupture takes place: Permeability of the sheared material may change abruptly, and it is beyond the scope of this study to investigate the hydrological consequence.

4 Results

Our model shows an average coefficient of pressurization of 0.115 MPa/°C for the Clay unit, given the material properties and the intertunnel distance. In Figure 2 the evolution of pressure and temperature at different times are presented.

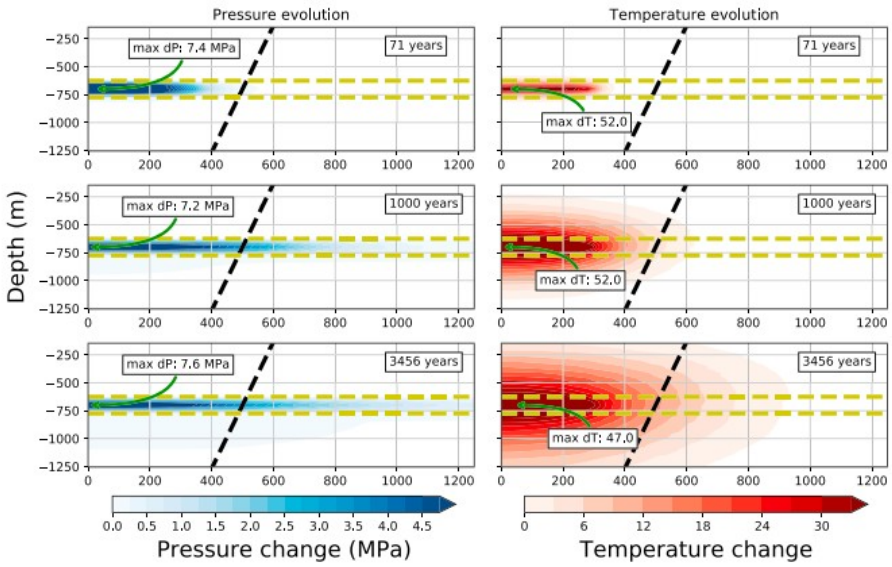

Figure 2. Forecasts of pressure and temperature changes around the emplacement tunnels at different times after emplacement, for a fault having 1-MPa cohesion (not rupturing). The value noted in the boxes are the maximum values not considering the tunnel element. Dashed yellow and black lines indicate, respectively, the Clay unit vertical extent and the fault zone. Color scales clipped. Different horizontal and vertical scales.

In this time interval, pressure and temperature increases away from the emplacement tunnels, gradually affecting a larger volume of rock mass. Two different boundaries can be broadly identified: a first one marking the clay rock formation affected by both temperature and pore pressure increases and a second one, extending vertically below and above the Clay formation, marking the volume affected almost exclusively by a temperature increase. The pore pressure increase of the clay formation by means of thermal pressurization is mitigated by the formations above and below having higher permeability: Pore pressure can propagate in the surrounding rock mass as shown already in Rutqvist, Zheng, et al. (2014). However, the most of the pore pressure perturbation is taking place in the Clay formation, due to its anisotropic permeability. The model shows no tensile failure occurrence in the rock mass due to the pressure increase.

The interaction of thermal pressurization, thermal diffusion, and pore pressure diffusion in the intratunnel rock mass gives already a complex pattern, with further nonlinearity given by the repressurization of the tunnels after their resaturation. While temperature in the tunnel is decreasing, at a distance temperature may increase. The increase in temperature may act on a rock mass already impacted by pressure diffusion, so the resulting increase in pressure is not thermal pressurization only, but the results of combination of time-dependent effects. These changes in pressure and temperature results in perturbation of local stress state, even at distance, due to the porothermoelastic response of the media. The relevance of these perturbations to fault stability can be computed in terms of change in Coulomb failure stresses (ΔCFS) on a failure plane determined by its dip and the shear direction. The CFS can be computed as

$$CFS = |\tau| + \mu(\sigma_n + p) - c_0, \quad (2)$$

where τ is the shear stress component along prescribed shear direction, σ_n is the normal stress acting perpendicular to that direction (negative compressive stress convention), and c_0 is the cohesion value. Variation of CFS will be positive if the plane is destabilized.

In Figure 3 ΔCFS is computed for a plane with a dip of 80 toward the repository, showing that the most relevant changes in CFS happens in proximity of the repository, in the underlying units.

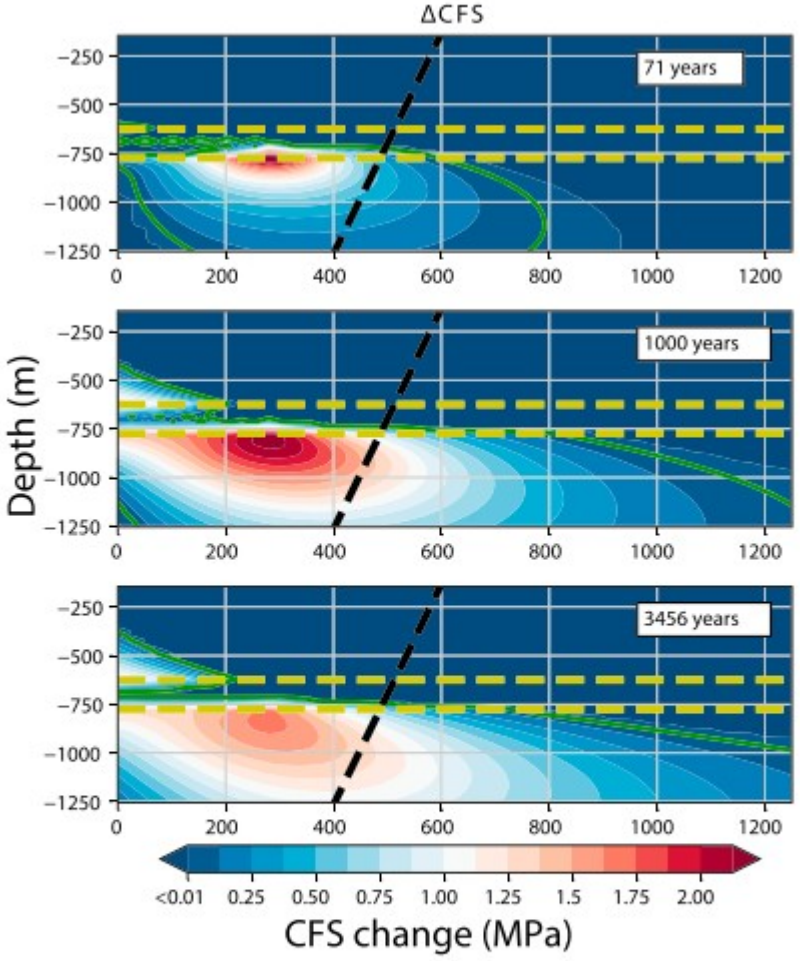

Figure 3. Distribution of positive changes in Coulomb failure stress (CFS), color scale clipped for clarity. Green line indicates the value 0.1 MPa; dashed yellow and black lines indicate the Clay unit vertical extent and the fault zone, respectively. Different horizontal and vertical scales.

With respect to stress state on the fault plane, although the fault plane is not affected by temperature change in the first centuries of operation, the pore pressure diffusion is quicker in reaching the fault plane and the stress state on the fault plane is strongly affected from the very beginning. With time progressing, the CFS values reaches an almost stable distribution, with minor

changes in its distribution after the first 1,000 years, although the pressure and temperature continue to diffuse.

We will consider as our basis scenario a setup where the stress ratio is 0.6, the distance between the fault plane and the outermost tunnel is 225 m and the initial cohesion is 0.35 MPa (dropping to 0 as soon as Mohr-Coulomb failure criterion is reached). Figure 4 shows in detail how a fault plane behaves in the basis scenario, in terms of pressure, stress changes, and fault slip evolution. Pore pressure changes on the fault plane are visible in detail in Figure 4a, while stress transfer effects, where pore pressure and temperature changes are indirectly affecting the stress state on the fault plane, are visible in Figure 4b. Additionally, in Figure 4b it is possible to note the increase in the fault strength. We refer to fault strength as the limiting shear stress value that the fault can sustain, that is, it is the sum of the frictional forces arising from effective normal stress acting on the fault and the cohesion of the fault itself. The fault strength is $\tau_s = c_0 - \mu(\sigma_n + p)$, where the symbols are the same as in equation 2 (the convention chosen is always stress is negative when compressive). For the fault section within the clay formation, the fault strength increase is due mostly to the increase in normal forces acting on the fault plane arising from the combined thermoelastic and poroelastic response: Being in line with the tunnels, the formation undergoes mostly a horizontal compressive strain, which in turn results in an increased compressive stress in the horizontal component. At rupture, the fault strength is reduced due to the prescribed cohesion loss (comparing the black lines, the shear stress matches the shear strength in Figure 4b where fault slip occurred, as plotted in Figure 4c).

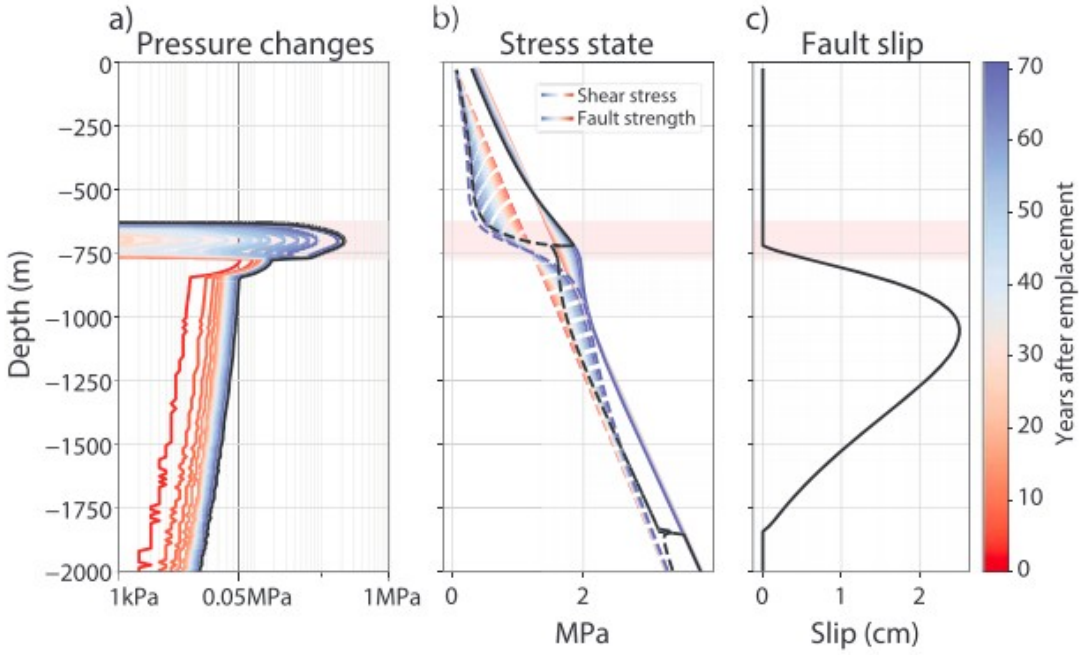

Figure 4. Evolution of pore pressure, stress, and slip for the basis scenario until rupture. Colored lines follow evolution; black lines depicts situation immediately after rupture. The light red area represents the clay formation vertical extent. Color code for the time is given on the very right in the diagram. (a) Pore pressure changes on the fault plane for the first 71 years after the emplacement of the canisters in the tunnels, logarithmic scale. (b) Evolution of shear stress (dashed line) and shear strength (solid line). Dark red line shows the initial stress state (maximum horizontal stress state 0.6 times the vertical lithostatic stress), while the blue lines shows the prefailure conditions. (c) Shear slip profile, maximum slip located below the nucleation zone, rupture breaking into the lower part of the Clay formation.

Results presented in Figure 3 and in Figure 4 show that reactivation of a normal fault (i.e., vertical stress is the largest) can take place, with the rupture nucleating at depth, between 250 and 900 m below the repository (between 950 and 1,600 m below surface) and during the first 1,000 years after emplacement. When rupture takes place, the fault ruptures for a length of about 1 km, with an average slip on the order of 1 cm.

For the basis scenario rupture conditions are reached at the time TR = 71 years after the emplacement of the canisters (assuming the canisters are set in place at the same time, in every tunnel). The rupture nucleates at a depth of 975 m, 275 m below the tunnels depth, and at a distance of 326 m from the outermost emplacement tunnel, well outside the zone affected by the thermal pressurization and by temperature change (Figure 2): Rupture does not correspond to the peak of pore pressure, neither in time (Figure 2) nor in location (Figure 4a). Indeed, the combined effect in terms of shear fault strength and shear stress acting on the fault is responsible for the reactivation. Although there is a large increase in pore pressure in the clay formation, the poroelastic response due to the pressurized region around the tunnel, combined with the thermoelastic response, is responsible for a net increase of fault strength in the clay formation, due to the resulting thermoporoelastic increase in horizontal stress component (Figure 4b), with

pore pressure diffusion reaching the fault plane only at a later time. The rupture length is visible in Figure 4c, where shear slip is shown, as well as by the black lines in Figure 4b, showing the fault section of about 1.1-km length that undergoes both shear stress and shear strength reduction, due to cohesion loss. The computed slip reaches a maximum of about 2.5 cm, with an average slip of 0.64 cm over the ruptured section of the fault (Figure 4c).

If the rupture releases its energy seismically, the scalar seismic moment M_0 would be $M_0 = G\overline{u}S$, with G representing the shear modulus, $\overline{u}$ the average slip, and S the ruptured area (Kanamori & Anderson, 1975). Seismic moment can then be translated into moment magnitude M_w, according to the relation $M_w = \frac{2}{3}\log_{10}M_0 - 6.07$ (Kanamori & Anderson, 1975). Assuming that the rupture happens on a circular patch, extending equally vertically and in the out of plane direction, the resulting magnitude M_w would be 2.98. This value is purely indicative and is given here as a first estimate of what can be the outcome of the reactivation of a certain fault given a certain stress state. Considering more advanced fault rheology (such as velocity-strengthening behavior and heterogeneous frictional properties) may change both the amount of slip and the ruptured area extent, with a resulting decrease in M_w that can be on the order of unit or more (Urpi et al., 2016).

The average slip on the fault is far less than the displacements that are expected at the surface or at the interface clay overburden (75 m above tunnels), which are due to the temperature and pressure change (Figure 5). Ground heave reaches a maximum of 7.5 cm already in the first 70 years after emplacement. These values are only indicative, and their limitations are acknowledged: Displacements may be overestimated (due to the plain-strain assumption), while the seismic magnitude calculation are heavily influenced by assumption on the out-of-plane rupture extent. Despite the uncertainty in the calculation, the vertical uplift is expected to be much larger than any natural tectonic process occurring in the same time frame. This displacement is occurring homogeneously over a wide area, with a maximum slope of about 0.02° for surface locations at 300-m distance from the center of the repository, corresponding to a deformation of less than 350 microstrains and therefore not affecting human made structure.

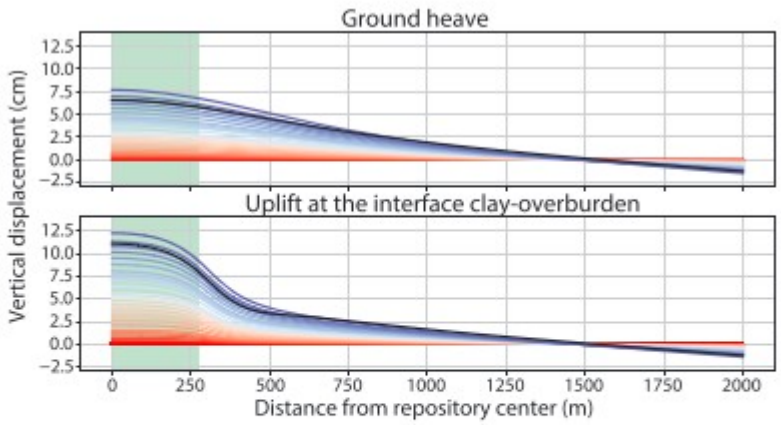

Figure 5. Vertical displacements induced by the repository and vertical scale (cm) greatly exaggerated with respect to horizontal scale (m). Light green area depicts the repository horizontal location. The distance is the in-line distance, calculated from the projection of the repository center on the surface under evaluation.

Dependency of slip and rupture area on the various parameters assumed for the model is presented in Figure 6. We performed a sensitivity analysis on stress ratio, lateral distance between the edge of the repository and the fault (tunnel-fault distance), and cohesion, in comparison to the base case presented in detail in Figure 4. Both ruptured length and average slip depend strongly on the stress ratio and less on fault properties and on the lateral between repository edge and the fault. The fault is not reactivated if the stress ratio between minimum horizontal and vertical stress is larger than 0.635. For a stress ratio S_h/S_v of 0.6, our analysis predicts that reactivation can occur, on a fault located up to 600 m away from the tunnels. With increasing distance between the tunnels and the fault, the reactivation is delayed: Figure 6b shows that for distances of 225 and 450 m rupture happens, respectively, 71 and 697 years after emplacement, but it gets larger as well, since at larger distance a bigger length of the fault is stressed. Figure 6c shows that cohesion of the fault modulates the rupture, with the largest rupture taking place for a value in between a cohesionless fault and a high cohesion (cohesion larger than 1 MPa). Displacements induced by the fault slip are order of magnitudes smaller that the displacements induced by thermal pressurization, unless the stress ratio is lower than 0.6: In that case the rupture will induce relevant deformations both in the Clay unit and at the surface.

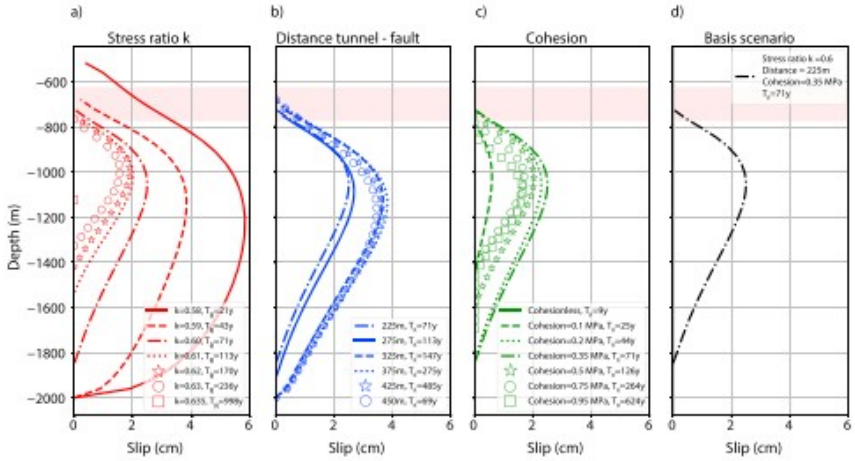

Figure 6. Rupture extent for different parameter variations. (a) Slip in dependence of stress ratio and indicates that a reduction of the ratio of minimum horizontal stress to vertical stress (reduction of k) increases the slip, with respect to the basis scenario. (b) Slip depending on fault-tunnel distance. (c) Slip magnitude with cohesion variations. (d) Basis scenario slip.

Slip and rupture extent are strongly influenced by the initial stress condition: In a worst-case scenario, where stress ratio is smaller than 0.59 (uniformly along the fault), rupture propagates through the Clay formation, even rupturing the overburden formation (Figure 6a, red solid line). Varying the fault distance affects the timing of the rupture but not the average slip nor the length of the ruptured fault section: The reactivation can occur even for a fault zone located more than 400 m from the edge of the repository (Figure 6b). Finally, the cohesion has also an impact on the amount of slip, rupture length, and reactivation time: For very low cohesion the fault is deforming plastically and continuously with little sudden slip at time of reactivation; if the cohesion is higher than 1 MPa, reactivation does not occur, while an intermediate cohesion value (0.2–0.35 MPa) allows for stress buildup that can be released suddenly (Figure 6c).

5 Discussion

This study presents a tectonic worst-case scenario, where a critically stressed fault is influenced by the THM changes caused by a nuclear waste repository located about 200 m away. The study focused on the imposed thermoporoelastic load destabilizing and leading to the slip of the weak surface. Due to the abundance of data collected in the Mont Terri Rock Laboratory (Bossart, Bernier, et al., 2017) we refer to similar conditions and hydromechanical properties, although our model does not aim at reproducing or predicting the geomechanical behavior of that specific site.

The increased temperature from the simulated decaying radioactive material contained in the emplacement tunnels is responsible for a rapid undrained increase in pressure in the host rock formation. The undrained response is by definition only an approximation of the condition of the media: In the case

presented here, the lower the ratio of fluid to thermal diffusivity is, the longer this approximation holds valid. At constant temperature, the pore pressure distributes in the repository formation and the surroundings, albeit slowly (the thermally induced pressure gradient will hamper the reequilibration of the pore pressure). The arising thermal pressurization can trigger fault reactivation, with conceptual similarities to the occurrence of fluid injection-induced seismicity, although here the time scale is much larger. A mitigation to the thermal pressurization effect may be provided by an increased permeability of the underlying units, which may be beneficial in terms of dissipating the thermal pore pressure and reducing the deformation, but it may negatively affect the stability of a fault located in the surrounding, providing a pathway for increased pressure to reach the lower, near-critically stressed sections of the fault, especially if the underlying unit is a fractured, low-porosity formation.

The nucleation patch for the scenario presented here is located at a depth of 975 m, 275 m below the emplacement tunnels. The nucleation of a rupture inside the hosting clay formation is extremely unlikely for a steeply dipping fault running through it: The combined stress perturbation due to temperature and pressure increase in the rock mass closer to the tunnels increases the minimum horizontal stress outside the heated and pressurized rock mass, clamping the fault and increasing its strength. When accounting also for the slip-strengthening behavior of the possible composition of fault gouge in a clay formation (Orellana et al., 2018), it is evident that the canisters emplacement should stabilize normal faults in the host formation. Accordingly, rheological studies show that a rupture nucleating in the argillaceous formation would be likely aseismic because of intrinsic velocity-strengthening behavior of clay-rich fault material saturated with water (Bakker et al., 2019; Tembe et al., 2010). In contrast, deeper sections of a normal fault may be destabilized by the combined effect of thermoelastic and poroelastic stress and by pore pressure increase. This is somewhat similar to previous thermal perturbation effects on fault stability (Segall & Fitzgerald, 1998) and to injection-induced fault reactivation studies (De Simone et al., 2017; Rutqvist et al., 2016) that showed how the pressurization of a certain rock mass volume influences the state of stress beyond this volume itself. Similar to the above-mentioned studies, it is possible to infer from our results that also normal fault reactivation could happen above the repository: In this case, shear stress changes depicted in Figure 4b would be reversed in sign, leading to the nucleation of rupture in the upper section of the fault. The occurrence of shearing of weakness plane located above the repository was numerically evaluated by Min et al. (2013), even by considering the stress transfer arising from temperature changes only: The poroelastic stress transfer arising from thermal pressurization enhances the thermoelastic effects.

From the excavation and the experiments performed at the Mont Terri underground research laboratory, it is known that an old, quiet, tectonic fault

is present in the Opalinus Clay formation. The fault existence is in apparent contrast with the Opalinus Clay formation properties that should present velocity-strengthening behavior (Orellana et al., 2018) and thus impeding the nucleation of a seismic rupture and the formation of such a structure. The aseismic behavior of a fault cutting through a clay formation has seen additional confirmation by the fluid injection experiment performed directly in the Opalinus Clay fault zone at the Mont Terri underground laboratory (Guglielmi et al., 2015). Therefore, the existence of a fault-like structure in a Clay formation is likely to be the result of a rupture nucleating elsewhere, possibly in a deeper formation with different rheology, which then propagated for a certain length through the Clay formation. For the specific case of the Mont Terri fault zones, the fault zones are interpreted as branch faults from basal shearing and the associated thrusting action (Bossart, Jaeggi, & Nussbaum, 2017). The velocity-strengthening behavior of a certain formation does not guarantee that a rupture nucleated below will not cut through the material. If that occurs, the amount of seismic energy released will not increase much, but the possibility of temporarily compromising the local sealing properties of the Clay material cannot be excluded.

The occurrence of induced seismicity in conjunction with the emplacement of high-level waste requires not only the presence of a fault but also that such a fault is under a near critical stress state for instability at least in some of its portion. This is not a trivial matter to exclude (or confirm). In the recent years, the occurrence of induced seismicity in the Central United States has been linked to the pressurization of the Arbuckle formation due to the disposal of waste water, with the seismic events generally located in the crystalline basement below the formation accommodating the injected fluid. Although this remote triggering of seismicity is possible either via a moderate increase in pore pressure or even just by poroelastic stress perturbation (Goebel et al., 2017), fault reactivation showed that the in situ stress conditions of the crust are much more heterogeneous than assumed, even for dormant tectonic settings (Levandowski et al., 2018).

The results of our model simulations show that a rupture may nucleate and propagate below the repository, even when the fault is located at a distance from the tunnel. The magnitude of such an event is limited by the size of the fault, and the actual rupture could be much less than the size of the fault. The slip calculated here is based on a 2-D representation. Previous studies, based on the same numerical tool applied here, have been used to quantify slip on a fault reactivated by fluid injection both in a 2-D plane-strain approximation (Rinaldi, Rutqvist, & Cappa, 2014) and in a 3-D model (Rinaldi et al., 2015), resulting in very similar magnitude estimates for the two cases.

The reactivation pattern shows that the stress changes on the fault plane are important for the buildup of a nucleation patch, while the size of the resulting rupture is mostly determined by the cohesion drop and the in situ stress state. Although there is a relation with fault-tunnel distance and rupture time, this relation breaks down if the stress transfer is not strong enough to

sustain the creation of a nucleation patch. For the basis scenario presented here, after the first 1,000 years the temperature and pore pressure change would continue diffusing, perturbing the stress state of a larger and larger volume: However, the magnitude of the perturbation at each point will peak at lower values, not affecting significantly the stability of a fault located farther than 600 m from the outermost tunnel. The possible tensile failure that may have occurred during the field test (according to Nguyen, 2018) is not occurring in our model. It must be noted that the field experiment happened at much shallower depth and the rock mass is weaker than the one expected to be found at depth.

Identifying tectonic structures and especially the in situ stress state in proximity of a target geological disposal site is therefore advised to confidently assess the likelihood of a reactivation scenario. We envision the importance of quantifying the generated ground motion in response to shallow event with $M_w > 3$, similarly to a previous study (Rutqvist, Cappa, et al., 2014), since the ground shaking acceleration and velocity values can be strongly affected by local conditions and by the reduced depth, while the predicted ground motion determined by historical regional tectonic events may not be completely applicable (Edwards et al., 2018).

6 Conclusions

For the conditions considered in this study of nuclear waste disposal in a low-permeability clay formation, the temperature increase imposed by the simulated heat releasing spent nuclear fuel contained in the canisters results in relevant changes in pore pressure. The simulation indicates that the formation hosting the disposal site is heated, up to 10–40 °C, and pressurized, up to 1–5 MPa, during the first centuries of operation of the repository. The simulations of a generic case showed how the combined stress transfer effect of thermoelastic and poroelastic stress change, with marginal contribution coming from the pore pressure diffusion, can create a nucleation patch of a seismic event on a fault located below the repository, outside the disposal formation. This may lead to the reactivation of a fault located at a lateral distance from the outermost tunnel on the order of hundreds of meters (up to 500 m), given a critical local stress ratio S_h/S_v (0.635 or less). Moreover, the simulations showed that reactivation is delayed with the increasing distance of the fault from the repository, but a delayed reactivation may rupture a slightly larger section of the weak structure, due to the thermal conduction resulting in a bigger volume of clay formation undergoing temperature changes. The thermoelastic and poroelastic response to temperature changes and thermal pressurization results then in an increased section of fault affected by a shear stress increase. Magnitude value and vertical uplift computed here are to be taken with caution and more as indicative of the order of magnitude rather than as exact values: Nonetheless, they show that the geological repository temperature and pressure will not pose a threat to the structural integrity of surface building and structures.

Given its practical implications, characterization of the in situ stress state and the possible presence of the faults not only in proximity of the geological storage site but also in the underlying formations is essential. The possibility of reactivating a fault by means of thermal pressurization depends not only on the relative position fault-repository but as well on the in situ stress state and on the hydromechanical properties of the underlying formation.

Acknowledgments

The authors would like to thank the reviewers Birgit Müller and Thomas Poulet for their feedback and valuable comments on the manuscript. The results of the numerical models can be downloaded from ETH repository, DOI 10.3929/ETHZ-B-000351237. This work has been carried out with the financial support from the Swiss Nuclear Safety Inspectorate (ENSI). A. P. Rinaldi is currently funded by SNSF Ambizione Energy Grant (PZENP2_160555). Funding to the Lawrence Berkeley National Laboratory was supported by the U.S. Department of Energy Contract DE-AC02-05CH11231.

References

Alonso, E. E., Gens, A., & Josa, A. (1990). A constitutive model for partially saturated soils. *Géotechnique*, 40(3), 405– 430. https://doi.org/10.1680/geot.1990.40.3.405

Bakker, E., Kaszuba, J., den Hartog, S., & Hangx, S. (2019). Chemo-mechanical behavior of clay-rich fault gouges affected by CO_2-brine-rock interactions. *Greenhouse Gases: Science and Technology*, 9(1), 19– 36. https://doi.org/10.1002/ghg.1831

Bock, H. (2001). *RA-experiment rock mechanics analysis and synthesis: Conceptual model of Opalinus Clay, TR 2001-3, Mont Terri Project*. Wabern, Switzerland: Federal Office of Topography (Swisstopo).

Bossart, P., Bernier, F., Birkholzer, J., Bruggeman, C., Connolly, P., Dewonck, S., Fukaya, M., Herfort, M., Jensen, M., Matray, J. M., Mayor, J. C., Moeri, A., Oyama, T., Schuster, K., Shigeta, N., Vietor, T., & Wieczorek, K. (2017). Mont Terri rock laboratory, 20 years of research: Introduction, site characteristics and overview of experiments. *Swiss Journal of Geosciences*, 110(1), 3– 22. https://doi.org/10.1007/s00015-016-0236-1

Bossart, P., Jaeggi, D., & Nussbaum, C. (2017). Experiments on thermo-hydro-mechanical behaviour of Opalinus Clay at Mont Terri rock laboratory, Switzerland. *Journal of Rock Mechanics and Geotechnical Engineering*, 9(3), 502– 510. https://doi.org/10.1016/j.jrmge.2016.11.014

Cappa, F., & Rutqvist, J. (2011). Modeling of coupled deformation and permeability evolution during fault reactivation induced by deep underground injection of CO_2. *International Journal of Greenhouse Gas Control*, 5(2), 336– 346. https://doi.org/10.1016/j.ijggc.2010.08.005

Cappa, F., & Rutqvist, J. (2012). Seismic rupture and ground accelerations induced by CO_2 injection in the shallow crust. *Geophysical Journal International*, 190(3), 1784– 1789. https://doi.org/10.1111/j.1365-246X.2012.05606.x

Cesca, S., Grigoli, F., Heimann, S., González, Á., Buforn, E., Maghsoudi, S., & Dahm, T. (2014). The 2013 September–October seismic sequence offshore Spain: A case of seismicity triggered by gas injection? *Geophysical Journal International*, 198(2), 941– 953. https://doi.org/10.1093/gji/ggu172

Chen, J., Niemeijer, A. R., & Fokker, P. A. (2017). Vaporization of fault water during seismic slip. *Journal of Geophysical Research: Solid Earth*, 122, 4237–4276. https://doi.org/10.1002/2016JB013824

Clarke, H., Eisner, L., Styles, P., & Turner, P. (2014). Felt seismicity associated with shale gas hydraulic fracturing: The first documented example in Europe. *Geophysical Research Letters*, 41, 8308– 8314. https://doi.org/10.1002/2014GL062047

Corkum, A. G., & Martin, C. D. (2007). The mechanical behaviour of weak mudstone (Opalinus Clay) at low stresses. *International Journal of Rock Mechanics and Mining Sciences*, 44(2), 196– 209. https://doi.org/10.1016/j.ijrmms.2006.06.004

De Simone, S., Carrera, J., & Vilarrasa, V. (2017). Superposition approach to understand triggering mechanisms of post-injection induced seismicity. *Geothermics*, 70, 85– 97. https://doi.org/10.1016/j.geothermics.2017.05.011

Deichmann, N., & Giardini, D. (2009). Earthquakes induced by the stimulation of an enhanced geothermal system below Basel (Switzerland). *Seismological Research Letters*, 80(5), 784– 798. https://doi.org/10.1785/gssrl.80.5.784

Diehl, T., Kraft, T., Kissling, E., & Wiemer, S. (2017). The induced earthquake sequence related to the St. Gallen deep geothermal project (Switzerland): Fault reactivation and fluid interactions imaged by microseismicity. *Journal of Geophysical Research: Solid Earth*, 122, 7272– 7290. https://doi.org/10.1002/2017JB014473

Edwards, B., Staudenmaier, N., Cauzzi, C., & Wiemer, S. (2018). A hybrid empirical Green's function technique for predicting ground motion from induced seismicity: Application to the Basel enhanced geothermal system. *Geosciences*, 8(5), 180. https://doi.org/10.3390/geosciences8050180

Garitte, B., Nguyen, T. S., Barnichon, J. D., Graupner, B. J., Lee, C., Maekawa, K., Manepally, C., Ofoegbu, G., Dasgupta, B., Fedors, R., Pan, P. Z., Feng, X. T., Rutqvist, J., Chen, F., Birkholzer, J., Wang, Q., Kolditz, O., & Shao, H. (2017). Modelling the Mont Terri HE-D experiment for the thermal–hydraulic–mechanical response of a bedded argillaceous formation to heating. *Environmental Earth Sciences*, 76(9), 345. https://doi.org/10.1007/s12665-017-6662-1

Gens, A., Sánchez, M., & Sheng, D. (2006). On constitutive modelling of unsaturated soils. *Acta Geotechnica*, 1(3), 137– 147. https://doi.org/10.1007/s11440-006-0013-9

Gens, A., Vaunat, J., Garitte, B., & Wileveau, Y. (2007). In situ behaviour of a stiff layered clay subject to thermal loading: Observations and interpretation. *Géotechnique*, 57(2), 207– 228. https://doi.org/10.1680/geot.2007.57.2.207

Ghabezloo, S., & Sulem, J. (2009). Stress dependent thermal pressurization of a fluid-saturated rock. *Rock Mechanics and Rock Engineering*, 42(1), 1–24. https://doi.org/10.1007/s00603-008-0165-z

Goebel, T. H. W., Weingarten, M., Chen, X., Haffener, J., & Brodsky, E. E. (2017). The 2016 Mw5.1 Fairview, Oklahoma earthquakes: Evidence for long-range poroelastic triggering at >40 km from fluid disposal wells. *Earth and Planetary Science Letters*, 472, 50– 61. https://doi.org/10.1016/j.epsl.2017.05.011

Guglielmi, Y., Cappa, F., Avouac, J.-P., Henry, P., & Elsworth, D. (2015). Seismicity triggered by fluid injection-induced aseismic slip. *Science*, 348(6240), 1224– 1226. https://doi.org/10.1126/science.aab0476

Horseman, S., Higgo, J., Alexander, J., & Harrington, J. (1996). *Water, gas and solute movement through argillaceous media. Nuclear Energy Agency Rep. CC-96/1*. Paris: OECD.

ITASCA Consulting Group, Inc. (2012) FLAC3D—Fast Lagrangian analysis of continua in three-dimensions, Ver. 5.0. Minneapolis.

Kanamori, H., & Anderson, D. L. (1975). Theoretical basis of some empirical relations in seismology. *Bulletin of the Seismological Society of America*, 65(5), 1073– 1095.

Levandowski, W., Herrmann, R. B., Briggs, R., Boyd, O., & Gold, R. (2018). An updated stress map of the continental United States reveals heterogeneous intraplate stress. *Nature Geoscience*, 11(6), 433– 437. https://doi.org/10.1038/s41561-018-0120-x

Martin, C. D., & Lanyon, G. W. (2003). Measurement of in-situ stress in weak rocks at Mont Terri Rock Laboratory, Switzerland. *International Journal of Rock Mechanics and Mining Sciences*, 40(7-8), 1077– 1088. https://doi.org/10.1016/S1365-1609(03)00113-8

Min, K.-B., Lee, J., & Stephansson, O. (2013). Implications of thermally-induced fracture slip and permeability change on the long-term performance of a deep geological repository. *International Journal of Rock Mechanics and Mining Sciences*, 61, 275– 288. https://doi.org/10.1016/j.ijrmms.2013.03.009

Monfared, M., Sulem, J., Delage, P., & Mohajerani, M. (2011). A laboratory investigation on thermal properties of the Opalinus Claystone. *Rock Mechanics and Rock Engineering*, 44(6), 735– 747. https://doi.org/10.1007/s00603-011-0171-4

Muñoz, J. J. (2007). Thermo-hydro-mechanical analysis of soft rock. Application to a large scale heating test and large scale ventilation test (Ph.D. Thesis). Universitat Politècnica de Catalunya. Retrieved from http://www.tdx.cat/handle/10803/6244

NAGRA (2008). Begründung der abfallzuteilung, der barrierensysteme und der anforderungen an die geologie. In *Nagra Technischer Bericht NTB 08-05* (p. 308). Nagra: Wettingen.

NAGRA (2016). *Projektkonzepte für die lagerkammern und Versieglungsstrecken und deren bewertung. Nagra Arbeitsbericht NAB 16-45*, (p. 262). Wettingen: Nagra.

Nguyen, S. T. (2018). Thermo-hydro-mechanical-chemical processes in geological disposal of radioactive waste—An example of regulatory research. *Advances in Geo-Energy Research*, 2(2), 173– 189. https://doi.org/10.26804/ager.2018.02.06

Orellana, L. F., Scuderi, M. M., Collettini, C., & Violay, M. (2018). Frictional properties of Opalinus Clay: Implications for nuclear waste storage: Frictional properties of Opalinus Clay. *Journal of Geophysical Research: Solid Earth*, 123, 157– 175. https://doi.org/10.1002/2017JB014931

Palciauskas, V. V., & Domenico, P. A. (1982). Characterization of drained and undrained response of thermally loaded repository rocks. *Water Resources Research*, 18(2), 281– 290. https://doi.org/10.1029/WR018i002p00281

Pruess, K., Oldenburg, C., & Moridis, G. (2012). *TOUGH2 user's guide, version 2.1, LBNL-43134(revised)*. Berkeley, California: Lawrence Berkeley National Laboratory.

Read, R. S. (2002). An approach to excavation design for a nuclear fuel waste repository: The thermal-mechanical stability study: Final report. Ontario Power Generation, Nuclear Waste Management Division.

Reid, M. E. (2004). Massive collapse of volcano edifices triggered by hydrothermal pressurization. *Geology*, 32(5), 373– 376. https://doi.org/10.1130/G20300.1

Rempel, A. W., & Rice, J. R. (2006). Thermal pressurization and onset of melting in fault zones. *Journal of Geophysical Research*, 111, B09314. https://doi.org/10.1029/2006JB004314

Rinaldi, A. P., Jeanne, P., Rutqvist, J., Cappa, F., & Guglielmi, Y. (2014). Effects of fault-zone architecture on earthquake magnitude and gas leakage related to CO_2 injection in a multi-layered sedimentary system. *Greenhouse Gases: Science and Technology*, 4(1), 99– 120. https://doi.org/10.1002/ghg.1403

Rinaldi, A. P., Rutqvist, J., & Cappa, F. (2014). Geomechanical effects on CO_2 leakage through fault zones during large-scale underground injection. *International Journal of Greenhouse Gas Control*, 20, 117– 131. https://doi.org/10.1016/j.ijggc.2013.11.001

Rinaldi, A. P., Vilarrasa, V., Rutqvist, J., & Cappa, F. (2015). Fault reactivation during CO_2 sequestration: Effects of well orientation on seismicity and leakage. *Greenhouse Gases: Science and Technology*, 5(5), 645– 656. https://doi.org/10.1002/ghg.1511

Rutqvist, J. (2017). An overview of TOUGH-based geomechanics models. *Computers & Geosciences*, 108, 56– 63. https://doi.org/10.1016/j.cageo.2016.09.007

Rutqvist, J., Cappa, F., Rinaldi, A. P., & Godano, M. (2014). Modeling of induced seismicity and ground vibrations associated with geologic CO_2 storage, and assessing their effects on surface structures and human perception, Int. *International Journal of Greenhouse Gas Control*, 24, 64– 77. https://doi.org/10.1016/j.ijggc.2014.02.017

Rutqvist, J., Rinaldi, A. P., Cappa, F., Jeanne, P., Mazzoldi, A., Urpi, L., & Vilarrasa, V. (2016). Fault activation and induced seismicity in geological carbon storage—Lessons learned from recent modeling studies. *Journal of Rock Mechanics and Geotechnical Engineering*, 8(6), 789– 804. https://doi.org/10.1016/j.jrmge.2016.09.001

Rutqvist, J., Rinaldi, A. P., Cappa, F., & Moridis, G. J. (2013). Modeling of fault reactivation and induced seismicity during hydraulic fracturing of shale-gas reservoirs. *Journal of Petroleum Science and Engineering*, 107, 31– 44. https://doi.org/10.1016/j.petrol.2013.04.023

Rutqvist, J., Rinaldi, A. P., Cappa, F., & Moridis, G. J. (2015). Modeling of fault activation and seismicity by injection directly into a fault zone associated with hydraulic fracturing of shale-gas reservoirs. *Journal of Petroleum Science and Engineering*, 127, 377– 386. https://doi.org/10.1016/j.petrol.2015.01.019

Rutqvist, J., Zheng, L., Chen, F., Liu, H.-H., & Birkholzer, J. (2014). Modeling of coupled thermo-hydro-mechanical processes with links to geochemistry associated with bentonite-backfilled repository tunnels in clay formations. *Rock Mechanics and Rock Engineering*, 47(1), 167– 186. https://doi.org/10.1007/s00603-013-0375-x

Schmitt, S. V., Segall, P., & Matsuzawa, T. (2011). Shear heating-induced thermal pressurization during earthquake nucleation. *Journal of Geophysical Research*, 116, B06308. https://doi.org/10.1029/2010JB008035

Segall, P., & Fitzgerald, S. D. (1998). A note on induced stress changes in hydrocarbon and geothermal reservoirs. *Tectonophysics*, 289(1-3), 117– 128. https://doi.org/10.1016/S0040-1951(97)00311-9

Sibson, R. H. (1973). Interactions between temperature and pore-fluid pressure during earthquake faulting and a mechanism for partial or total stress relief. *Nature Physical Science*, 243(126), 66– 68. https://doi.org/10.1038/physci243066a0

te Kamp, L., & Konietzky, H. (2005). Numerical modelling of the thermo–hydro–mechanical loading in a geological repository for HLW and SF (No. Arbeitsbericht NAB 09-25).

Tembe, S., Lockner, D. A., & Wong, T.-F. (2010). Effect of clay content and mineralogy on frictional sliding behavior of simulated gouges: Binary and ternary mixtures of quartz, illite, and montmorillonite. *Journal of Geophysical Research*, 115, B03416. https://doi.org/10.1029/2009JB006383

Urpi, L., Rinaldi, A. P., Rutqvist, J., Cappa, F., & Spiers, C. J. (2016). Dynamic simulation of CO_2-injection-induced fault rupture with slip-rate dependent friction coefficient. *Geomechanics for Energy and the Environment*, 7, 47–65. https://doi.org/10.1016/j.gete.2016.04.003

Wileveau, Y. (2005). *THM behaviour of host rock (HE-D experiment): Progress report September 2003–October 2004, Part 1 Mont Terri Technical Report TR 2005-03*. Wabern, Switzerland: Federal Office of Topography (Swisstopo).

Xu, B., Yuan, Y., & Yang, B. (2013). *Impact of thermal pore pressure on the caprock integrity during the SAGD operation. In SPE-165448-MS*. Alberta, Canada: SPE: Society of Petroleum Engineers. https://doi.org/10.2118/165448-MS

Zbinden, D., Rinaldi, A. P., Urpi, L., & Wiemer, S. (2017). On the physics-based processes behind production-induced seismicity in natural gas fields. *Journal of Geophysical Research: Solid Earth*, 122, 3792– 3812. https://doi.org/10.1002/2017JB014003

Zhang, C.-L., Conil, N., & Armand, G. (2017). Thermal effects on clay rocks for deep disposal of high-level radioactive waste. *Journal of Rock Mechanics and Geotechnical Engineering*, 9(3), 463– 478. https://doi.org/10.1016/j.jrmge.2016.08.006